Structure
Article

Structure and Function of an ADP-Ribose-Dependent Transcriptional Regulator of NAD Metabolism

Nian Huang,[1,6] Jessica De Ingeniis,[2,3,6] Luca Galeazzi,[2] Chiara Mancini,[2] Yuri D. Korostelev,[4] Alexandra B. Rakhmaninova,[4,5] Mikhail S. Gelfand,[4,5] Dmitry A. Rodionov,[3,5] Nadia Raffaelli,[2,*] and Hong Zhang[1,*]
[1]Department of Biochemistry, University of Texas Southwestern Medical Center, Dallas, TX 75390, USA
[2]Department of Molecular Pathology and Innovative Therapies, Section of Biochemistry, Università Politecnica delle Marche, 60131 Ancona, Italy
[3]The Burnham Institute for Medical Research, La Jolla, CA 92037, USA
[4]Faculty of Bioengineering and Bioinformatics, Moscow State University, Moscow 119992, Russia
[5]Institute for Information Transmission Problems, Russian Academy of Sciences, Moscow 127994, Russia
[6]These authors contributed equally to this work
*Correspondence: zhang@chop.swmed.edu (H.Z.), n.raffaelli@univpm.it (N.R.)
DOI 10.1016/j.str.2009.05.012

SUMMARY

Besides its function as an essential redox cofactor, nicotinamide adenine dinucleotide (NAD) also serves as a consumable substrate for several reactions with broad impact on many cellular processes. NAD homeostasis appears to be tightly controlled, but the mechanism of its regulation is little understood. Here we demonstrate that a previously predicted bacterial transcriptional regulator, NrtR, represses the transcription of NAD biosynthetic genes in vitro. The NAD metabolite ADP-ribose functions as an activator suppressing NrtR repressor activity. The presence of high ADP-ribose levels in the cell is indicative of active NAD turnover in bacteria, which could signal the activation of NAD biosynthetic gene expression via inhibiting the repressor function of NrtR. By comparing the crystal structures of NrtR in complex with DNA and with ADP-ribose, we identified a "Nudix switch" element that likely plays a critical role in the allosteric regulation of DNA binding and repressor function of NrtR.

INTRODUCTION

Nicotinamide adenine dinucleotide (NAD) is an indispensable cofactor in all living organisms. In addition to its fundamental function in hundreds of cellular redox reactions, NAD is also a substrate of a number of nonredox enzymes such as bacterial DNA ligase (Wilkinson et al., 2001), various ADP-ribosyltransferases (Holbourn et al., 2006; Koch-Nolte et al., 2008), and protein deacetylases of Sirtuin/CobB family (Denu, 2005; Frye, 2000; Marmorstein, 2004). Depletion of the NAD(P) pool as well as accumulation of certain intermediates, such as quinolinic acid and pyridine mononucleotides, is harmful to the cell. Therefore, biosynthesis and homeostasis of NAD is believed to be a subject of tight regulation. In recent years the NAD biosynthesis machineries, consisting of various de novo synthesis, salvage, and recycling pathways, have been elucidated in the majority of eukaryotic and prokaryotic species using approaches that combine comparative genomic analysis, metabolic pathways reconstruction, and experimental characterization (Begley et al., 2001; Belenky et al., 2009; Imai, 2009; Magni et al., 2004; Tempel et al., 2007). However, the mechanisms underlying cellular NAD regulation in response to various physiological and environmental conditions are poorly understood. Until recently, two transcriptional factors (TFs) of NAD biosynthesis were known in a limited number of bacterial species: the multifunctional NadR in *Enterobacteria* acts as a NAD-dependent repressor of de novo and salvage NAD biosynthesis genes (Gerasimova and Gelfand, 2005; Grose et al., 2005; Holley et al., 1985), while YrxA (later renamed NiaR), found in most *Bacillus*/*Clostridium* species as well as *Fusobacteria* and *Thermotogales*, represses the transcription of certain NAD biosynthetic genes in response to elevated nicotinic acid levels (Rodionov et al., 2008b; Rossolillo et al., 2005). In an effort to uncover new potential transcriptional regulators of NAD metabolism in bacteria, we applied comparative genomic techniques to analyze NAD biosynthesis subsystems in more than 400 bacterial species and identified a novel TF family, the Nudix-related transcriptional regulators (NrtR), in a wide range of bacteria lacking NadR and NiaR (Rodionov et al., 2008a). Comparative genomics-based identification of the NrtR-binding DNA motifs (termed NrtR boxes) allowed in silico reconstruction of NrtR regulons that primarily include genes involved in various aspects of NAD metabolism (Rodionov et al., 2008a). Structural information of two NrtR proteins (PDB codes 2fml and 2fb1) have recently been obtained by the Midwest Center for Structural Genomics and revealed that NrtR consists of an N-terminal Nudix hydrolase-like domain (Bessman et al., 1996) and a C-terminal winged helix-turn helix (wHTH) domain that is distantly related to histone H5 and several large families of bacterial transcription factors (Aravind et al., 2005; Ramakrishnan et al., 1993). While the wHTH domain of NrtR is predicted to bind to the operator site of its regulated genes, the Nudix domain is presumably responsible for specific binding of an effector molecule. Among various Nudix hydrolases, ADP-ribose (ADPR) pyrophosphatase (ADPRase), catalyzing ADPR hydrolysis to AMP and ribose 5-phosphate, shows the most significant similarity to the Nudix domain of NrtR proteins (Rodionov et al., 2008a). Notably, the Nudix domain in most NrtR family

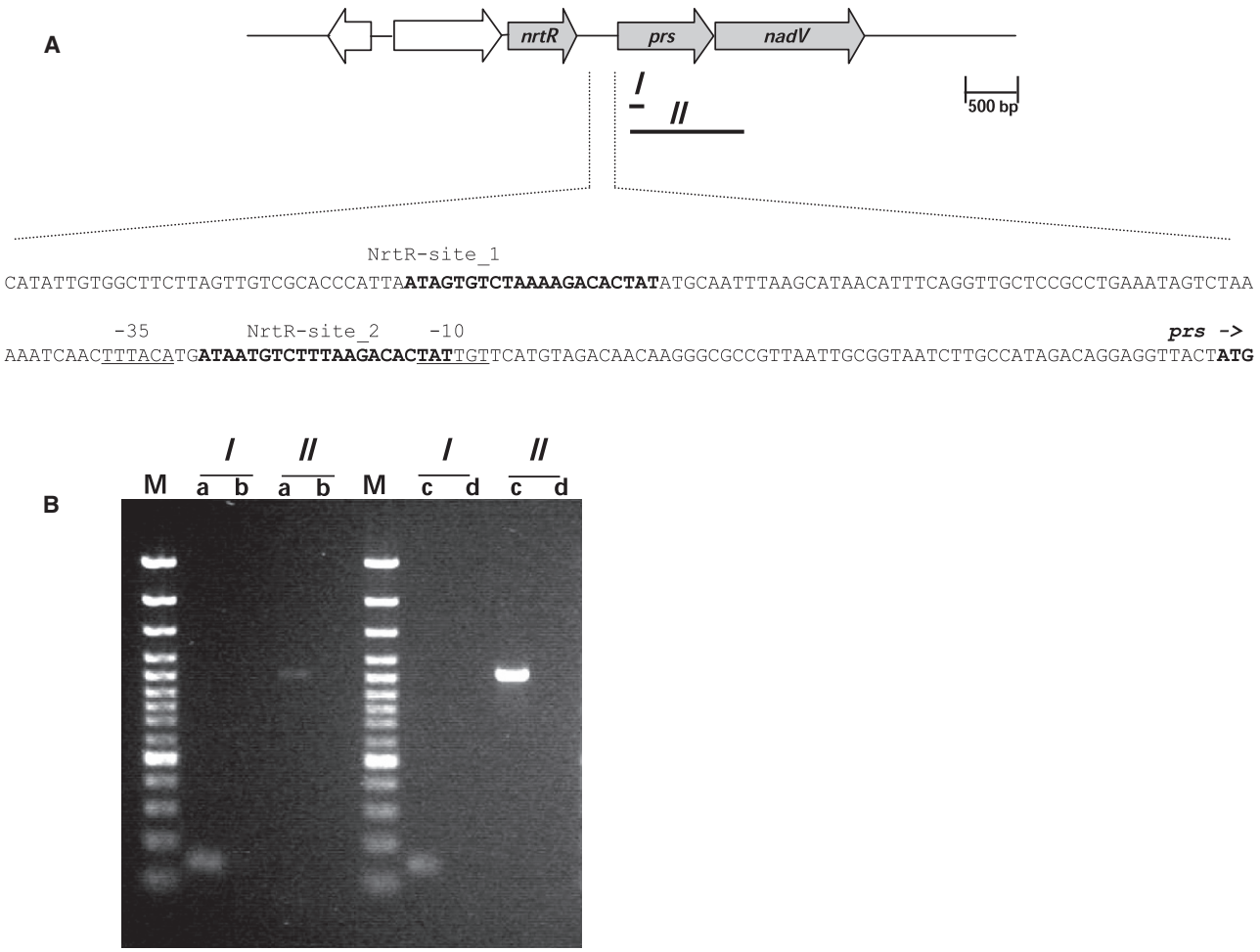

Figure 1. Transcriptional Analysis of the *nrtR-prs-nadV* Region

(A) Schematic representation of *nrtR*, *prs*, and *nadV* genes on the *S. oneidensis* chromosome and the promoter region of the *prs-nadV* operon. I and II represent the PCR-amplified fragments. In the promoter region sequence the two predicted NrtR-binding sites are in bold, the putative −10 and −35 regulating sequences are underlined, and the start codon of *prs* is indicated by an arrow and shown in boldface.

(B) Ethidium bromide-stained agarose gel showing the PCR products obtained with cDNA (lanes a), RNA (lanes b), genomic DNA (lanes c), and water (lanes d) as the templates and the primer pairs amplifying fragments I and II. Lanes M, 1 kb DNA ladder.

members is predicted to be catalytically inactive, as several active site residues in the Nudix motif and L9 loop regions are no longer conserved (see Figure S1 available online). It appears that the ancient Nudix hydrolase domain was recruited by NrtR to function as a signaling module and might have lost its enzymatic activity but retained the ability to bind (and hence to be regulated by) ADPR, the product of NAD glycohydrolytic reaction.

Here we report the functional and structural characterization of NrtR from a model bacterium, *Shewanella oneidensis* (*so*NrtR). We demonstrate by an in vitro transcriptional assay that *so*NrtR is indeed an ADPR-dependent transcriptional repressor. The surprisingly high content of ADPR in the cell (0.8 mM; see Results) is indicative of active NAD degradation processes in bacteria, of which very little is currently known. We present the structures of *so*NrtR in complex with specific NrtR box DNA and with ligand ADPR. These structures allowed identification of a ''Nudix switch'' structural element that transduces an ADPR-binding signal to the DNA-binding domain of *so*NrtR.

RESULTS

Organization and Transcriptional Analysis of the *nrtR-nadV-prs* Region in *S. oneidensis* Genome

The *nrtR* gene is clustered with genes *prs* and *nadV* on the *S. oneidensis* chromosome, and two NrtR-binding sites were predicted in the intergenic region between *nrtR* and *prs* (Rodionov et al., 2008a) (Figure 1A). The *prs* gene encodes the enzyme ribose phosphate pyrophosphokinase that synthesizes phosphoribosyl pyrophosphate (PRPP), a central precursor for the synthesis of nucleotides (including NAD) and amino acids. The *nadV* gene encodes the enzyme nicotinamide (Nam) phosphoribosyltransferase that catalyzes the transfer of the phosphoribosyl moiety of PRPP to Nam, forming NMN, the direct NAD precursor. The *nadV* gene is positioned 10 bp downstream of *prs* and oriented in the same direction. To investigate whether they form a transcriptional unit, RNA isolated from cells was reverse transcribed and the resulting cDNA was used as a

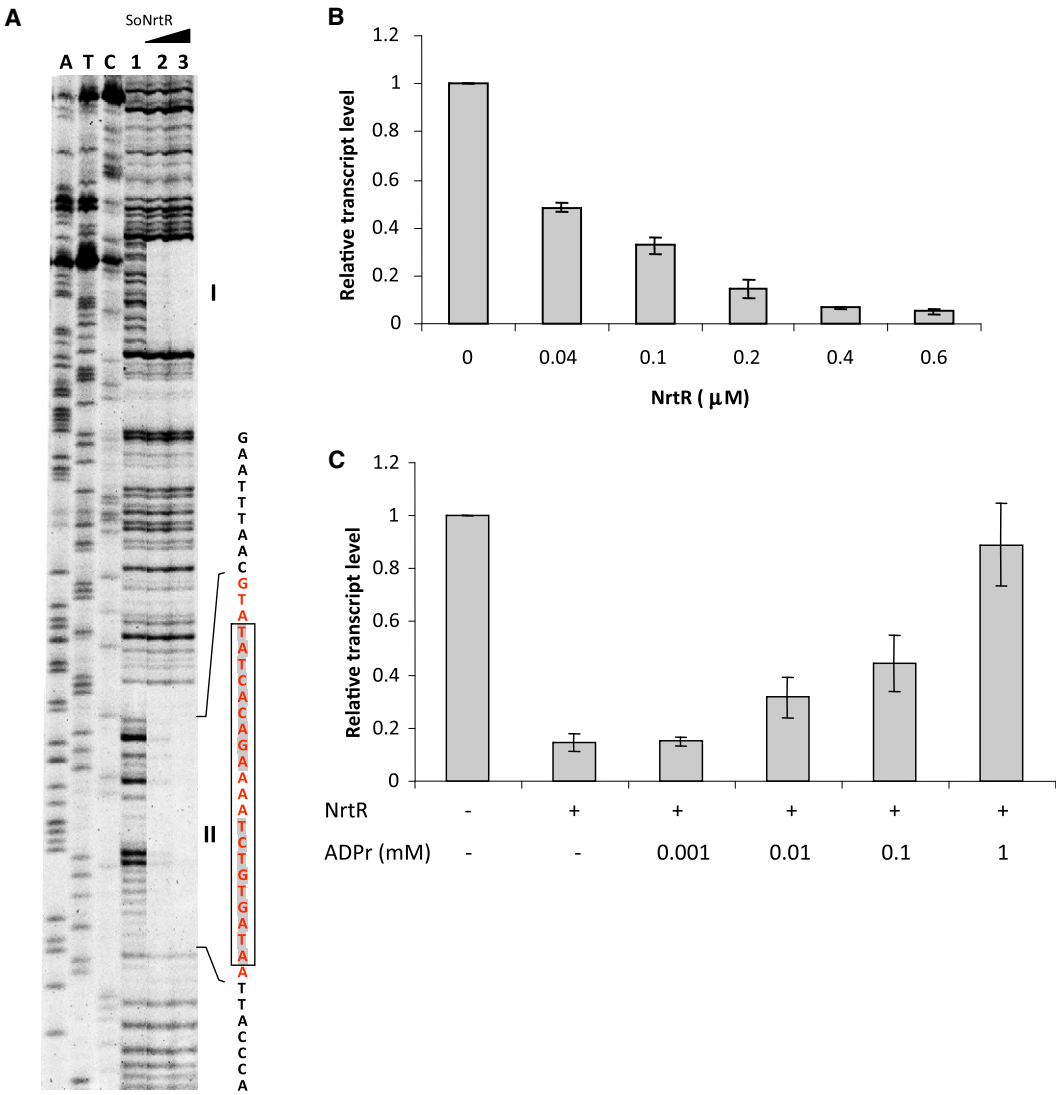

Figure 2. DNase I Footprinting and In Vitro Transcription Assay

(A) DNase I footprinting of *so*NrtR on *prs-nadV* operator DNA. Lanes marked A, T, and C are from a DNA-sequencing ladder of the coding strand of the 144-bp *prs-nadV* operator DNA. The remaining lanes show the results of DNase I footprinting. Lane 1 contains no *so*NrtR; lanes 2 and 3 contain increasing amounts of *so*NrtR. The DNA sequence around the second protected region is shown to the right of the gel. Bases protected against DNase I treatment are colored red. The 21 bp NrtR box sequence is boxed.

(B) *prs-nadV* transcript levels determined by real-time PCR in the presence of various amounts of NrtR.

(C) *prs-nadV* transcript levels in the presence of 0.2 μM NrtrR and increasing amounts of ADPR. Levels of transcripts were normalized to the level in the absence of *so*NrtR (B) and ADPR (C). For the relative quantification $2^{-\Delta Ct}$ was calculated for each sample (ΔCt being the difference between the Ct values of the target and the normalizer). Data represents the averaged results from three independent experiments with duplicates; vertical bars represent standard deviations.

template in PCR with specific primers amplifying the region encompassing *prs* and part of *nadV* (region II in Figure 1A). Amplification of region I in the *prs* gene was also performed as a positive control. Additional PCR controls use genomic DNA and RNA as templates. Amplification of the intergenic region II with cDNA as the template establishes that *prs* and *nadV* genes are transcribed as one mRNA molecule (Figure 1B).

NrtR Is a Transcriptional Repressor

We have previously shown that *so*NrtR specifically binds to DNA derived from the promoter region of *prs-nadV* operon containing two predicted NrtR-boxes (Rodionov et al., 2008a). A fluorescence-based DNase I footprinting assay confirmed that the predicted *so*NrtR boxes are protected from DNase I digestion in the presence of *so*NrtR (Figure 2A). One of the two *so*NrtR-binding sites is located between the predicted promoter elements and partially overlaps the −10 box (Figure 1A), strongly suggesting that NrtR may act as a transcriptional repressor. To confirm this hypothesis, the effect of NrtR on *prs-nadV* transcription was tested in vitro with σ^{70}-saturated RNA polymerase from *E. coli* and a linear DNA template consisting of the promoter region and the 5′ end of the *prs* gene. The resulting transcript

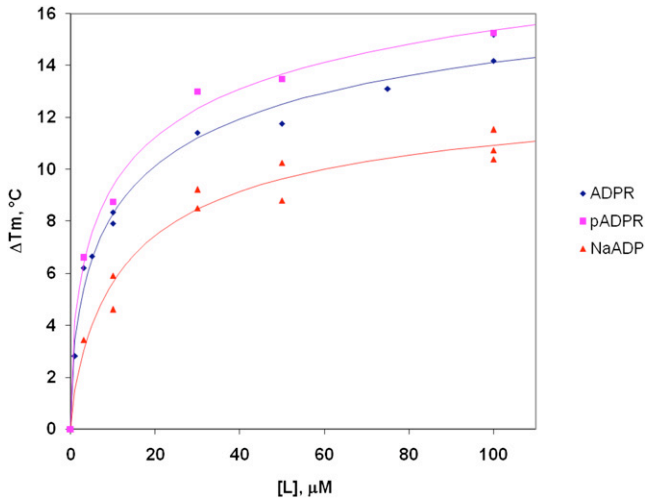

Figure 3. Effects of ADPR, pADPR, and NaADP on the Thermal Stability of *so*NrtR

The increase in the thermal stability (ΔT_m) of NrtR was monitored in the presence of varying concentrations of ADPR, pADPR, and NaADP.

was quantified by reverse transcription-mediated real-time PCR. As shown in Figure 2B, transcription was repressed by NrtR in a dose-dependent manner. An unrelated operon was used as a control to verify the specificity of the NrtR effect. The Ct values for the control gene in the absence and presence of 0.2 μM *so*NrtR were 16.1 ± 0.08 and 15.2 ± 0.03, respectively. These results indicate that *so*NrtR specifically represses in vitro transcription of the *prs-nadV* operon.

NAD Metabolites (p)ADPR and NaADP Are Effectors of NrtR

Several evidences, including mobility shift assay data and sequence and structure similarity between the NrtR Nudix domain and ADPRases, suggest that ADPR is the most likely effector molecule of NrtR (Rodionov et al., 2008a). We tested the effect of ADPR on NrtR transcriptional repression by performing the in vitro transcription assay in the presence of various amounts of the metabolite. As shown in Figure 2C, ADPR was able to reverse the repressive effect of *so*NrtR in a dose-dependent manner. Repression of transcription was fully abolished in the presence of 1 mM ADPR. The same effect was also observed with 1 mM phospho-ADPR (pADPR) and NaADP, while other NAD-related metabolites, ADP, ribose 5-phosphate, NAD, NADP, NaAD, NADH, NADPH, Nam, NMN, and PRPP (at 1 mM concentration) did not show any significant effect on the repressive activity of NrtR (data not shown).

The binding affinities of NAD metabolites to NrtR were determined using a fluorescence-based thermal unfolding assay (Pantoliano et al., 2001). NAD metabolites that do not affect NrtR-DNA interaction and NrtR-repressive activity did not significantly affect NrtR thermal stability (data not shown). In contrast, protein thermal stability (ΔT_m) markedly increased with increasing concentrations of ADPR, pADPR, and NaADP (Figure 3). The titration profiles resemble saturation kinetic profiles, indicating that these molecules bind specifically. Binding affinities (K_d) of 17.9, 17.7, and 15.4 μM were obtained for ADPR, pADPR, and NaADP, respectively (Figure 3).

To assess how *so*NrtR repressor function may be affected by cellular ADPR levels, we determined the concentration of ADPR in *S. oneidensis* cells. Direct HPLC analysis of cell extracts revealed one single peak (0.97 purity index) that increased in an ADPR spiked sample (Figure 4). Its identity as genuine ADPR was confirmed by coelution with an ADPR standard (Figure 4, arrow), identical UV absorption spectra of the sample peak and ADPR standard (data not shown), and disappearance of the peak after incubation with nucleotide pyrophosphatase (Figure 4, inset). From a comparison of the peak areas of the unspiked and spiked samples, a recovery of about 98% during sample preparation was calculated. ADPR in *S. oneidensis* cells was corrected for recovery and normalized to cell volume, resulting in 1.3 ± 0.2 mM. Control experiments ruled out a possible degradation of NAD to ADPR during sample preparation, but showed that NADH is completely hydrolyzed to ADPR under the experimental condition (data not shown). The same observation was also reported by others recently (Tong et al., 2009). Therefore NADH concentration was measured in *S. oneidensis* cells as described in Experimental Procedures, resulting in

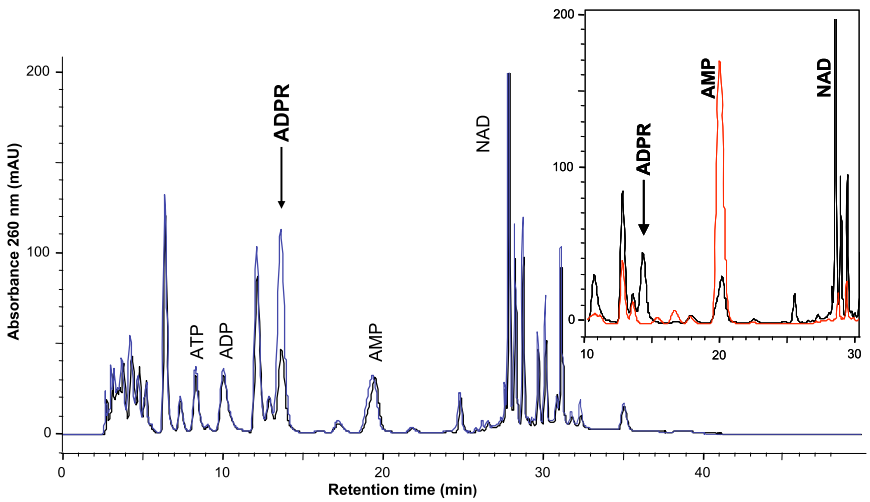

Figure 4. ADPR Content in *S. oneidensis* Cells

HPLC chromatograms of unspiked *S. oneidensis* extract (black line) and ADPR spiked extract (blue line). Inset shows part of the chromatogram of the unspiked extract (black line) in comparison with that of the same extract after incubation with nucleotide pyrophosphatase (red line).

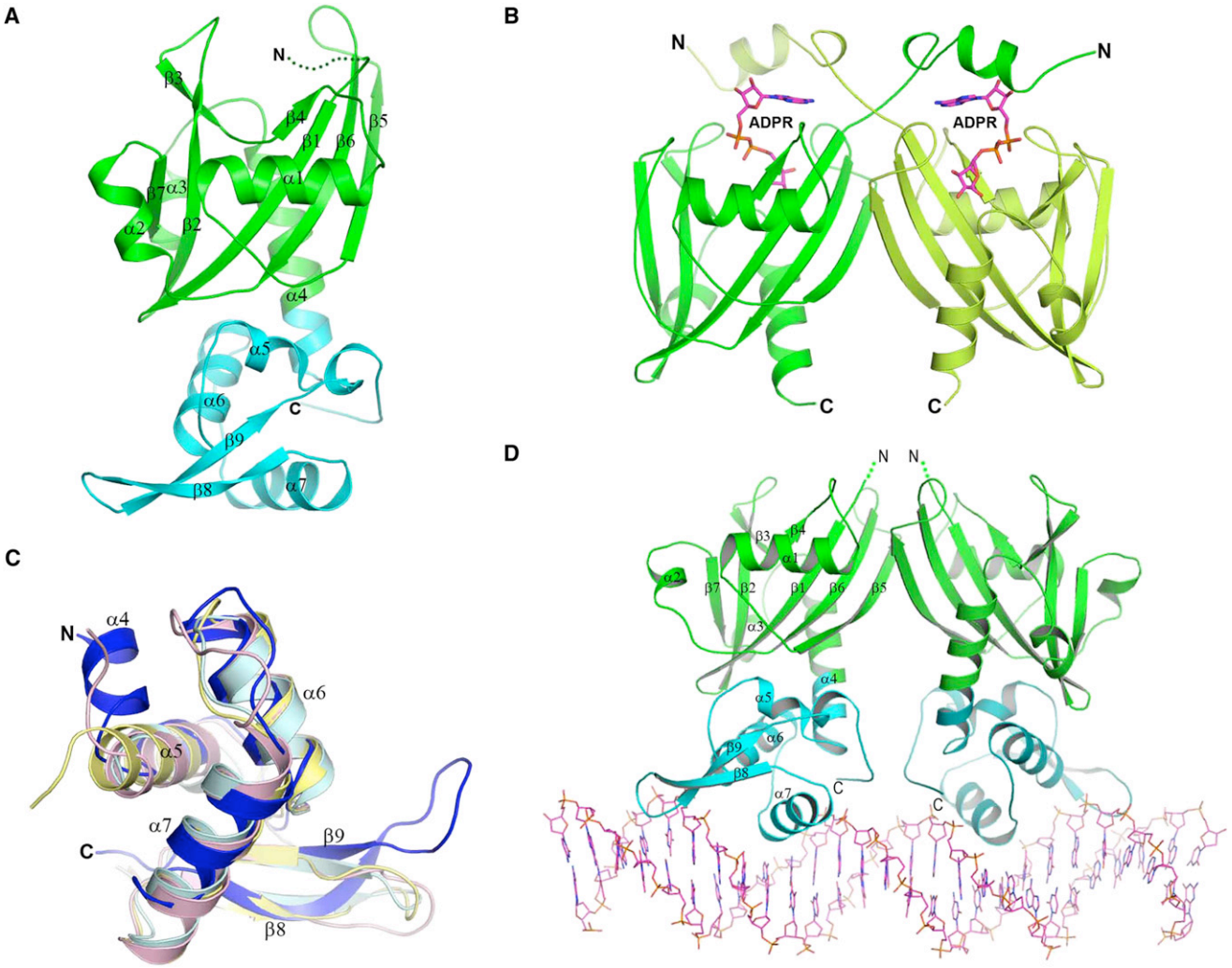

Figure 5. Structures of *so*NrtR and Its Complexes with DNA and Effector ADPR

(A) Ribbon presentation of *so*NrtR monomer with the Nudix domain colored in green and wHTH domain in cyan. The secondary structure elements (strands β1–β9 and helices α1–α7) are labeled. The disordered N-terminal region is indicated by dots.

(B) Structure of *so*NrtR N-terminal Nudix domain dimer in complex with ADPR. ADPR molecules are shown as magenta sticks.

(C) Superposition of *so*NrtR wHTH domain (blue) with histone H5 (pink; PDB code 1hst), penicillinase repressor (light cyan; 1sd4), and ferric uptake regulator (yellow; 1mzb).

(D) Structure of full-length *so*NrtR dimer in complex with DNA. The protein is presented as ribbons and DNA as sticks.

0.5 ± 0.04 mM. Endogenous ADPR concentration is thus estimated to be 0.8 ± 0.16 mM, after subtracting NADH concentration from the total ADPR. Cellular levels of these nucleotides, as well as of NAD, ATP, and ADP, are summarized in Table S2.

Overall Structure of NrtR

We have determined the structures of apo *so*NrtR at 2.2 Å resolution and in complex with a 28 nt NrtR box DNA duplex at 2.9 Å resolution. However, repeated attempts to obtain cocrystals of full-length *so*NrtR in complex with ADPR were not successful. We therefore determined the structure of the N-terminal domain of *so*NrtR (residue 1–159) in complex with ADPR (referred to as *so*NrtR_N-ADPR) at 2.4 Å resolution.

The overall structure of *so*NrtR monomer contains two domains (Figure 5A). The N-terminal domain displays the Nudix hydrolase-like fold and is most closely related to the ADPRase domain of bacterial NadM-Nudix protein (Huang et al., 2008) with a sequence identity of ~27% and root mean square deviation (rmsd) between C_α positions of 1.6 Å. The *so*NrtR Nudix domain contains a central mixed five-strand β sheet comprised of β7, β2, β1, β6, and β5, with four α helices (α1–α4) packed on both sides of the sheet (Figure 5A). The long α4 helix, containing 16 residues, connects the Nudix domain to the C-terminal wHTH DNA-binding domain.

*so*NrtR forms homodimers in solution (data not shown) and in crystals through Nudix domain interactions (Figure 5B). Similar to NadM_Nudix proteins (Huang et al., 2008), *so*NrtR dimerizes mainly through a partial stacking of the central β sheet from each subunit (Figure 5B). This dimerization mode is very different from the more distantly related single domain bacterial ADPRases,

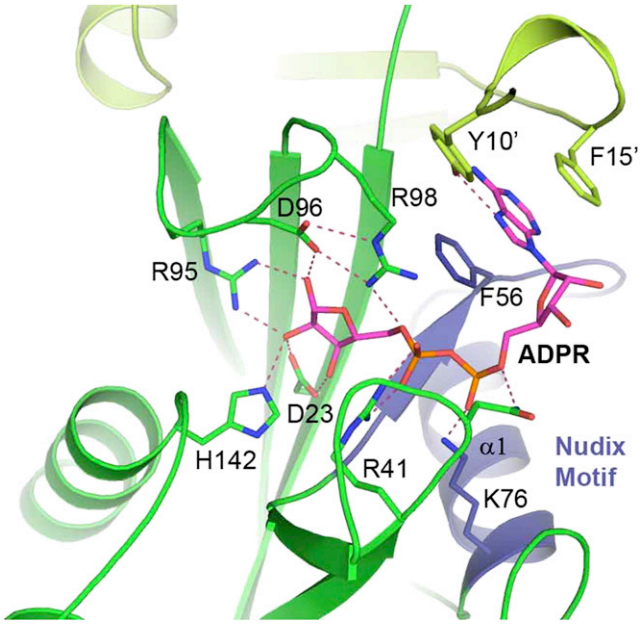

Figure 6. Effector-Binding Site of *so*NrtR
The bound ADPR (magenta) and interacting protein side chains are shown as sticks. Hydrogen bonds are indicated by dashed lines. Residues from the second monomer are colored in pale green and Nudix Motif region is colored blue.

where dimer interface is composed mostly of a C-terminal α helix (corresponding to α4 of *so*NrtR) and a N-terminal three-stranded β sheet domain that is lacking in *so*NrtR. The N-terminal 18 residues of *so*NrtR are disordered in the apo and *so*NrtR-DNA complex structures, but become well ordered upon ADPR binding (Figure 5B). These residues are structured into a short α helix, which is swapped between the two subunits of *so*NrtR dimer, forming a lid over the bound ADPR (see below for more details).

The DNA-binding wHTH domain of *so*NrtR consists of a three-helical bundle (α5, α6, and α7) followed by a long β hairpin "wing" (β8 and β9) (Figure 5C). Structure similarity search using Dali server (Holm and Sander, 1995) identified histone H5 (PDB code 1hst) (Ramakrishnan et al., 1993), penicillinase repressor (1sd4) (Safo et al., 2005), and ferric uptake regulator (1mzb) (Pohl et al., 2003) as the closest structural neighbors. While the relative positioning of secondary structure elements in *so*NrtR wHTH are similar to these other wHTH domains, there are significant variations in the lengths and conformations of the connecting loops (Figure 5C). In particular, the β hairpin wing in *so*NrtR is much longer than the other wHTH proteins and extended toward a different orientation.

Effector-Binding Site of NrtR

The details of *so*NrtR ligand-binding site are revealed in its complex structure with ADPR (Figure 6), which are very similar to those observed in NadM_Nudix proteins but different from other bacterial ADPRases (Huang et al., 2008). The adenine ring of ADPR is sandwiched between the side chains of Phe56 from one subunit and Phe15' from the second subunit of the dimer. The side chain hydroxyl of Tyr10', also from the second subunit, is hydrogen bonded to both N6 amino and N7 nitrogen groups of the adenine. The positively charged residues Arg41, Lys76, and Arg98 form salt bridges with the oxygen of the diphosphates of ADPR. An extensive hydrogen bonding network exists between the protein and the hydroxyl groups of the ADPR terminal ribose, involving residues Asp23, Arg95, Asp96, and His142 (Figure 6). Since there is no direct interaction between *so*NrtR and the adenylyl ribose group, modification at the ribose O2′ position, such as O2′-pADPR, should bind to the protein equally well. This observation is fully consistent with the results from the *so*NrtR ligand-binding assays described in the previous section.

Since the ligand-binding assays revealed that NaADP, the product of NADP base-exchange reaction, binds to *so*NrtR with a similar affinity as ADPR, we modeled a NaADP molecule in the *so*NrtR ligand-binding site (Figure S2). The ADPR moiety was modeled to occupy the same position as the ADPR. The presence of the additional nicotinate base would require that the loop between strand β5 and β6 (residues 92–101) adopt a slightly more open conformation similar to that in the apo *so*NrtR structure. Residue Phe140 would form a stacking interaction with the pyridine ring and Arg98 may interact with the exocyclic carboxyl group (Figure S2).

NrtR Recognizes DNA Through Its wHTH Motif

The crystallographic asymmetric unit of the *so*NrtR-DNA complex contains one *so*NrtR dimer bound to a 28 nt NrtR box DNA (Figure 5D). The conformations of the two monomers in the DNA-bound *so*NrtR dimer are essentially identical (rmsd of 0.22 Å for all C_α atoms) and are also very similar to that of apo *so*NrtR (rmsd 0.61 Å), except that the wing β hairpin is better ordered in the complex than in the apo *so*NrtR structure, apparently through interactions with DNA. In the DNA complex crystal structure, the first 5′-overhanging nucleotide, *Cyt1* (and *Cyt1'*), is disordered, while the base-paring 27 nt are clearly visible in the electron density (Figure S3). (The prime mark denotes the nucleotide in the complementary strand.) The end base pairs, *Gua2-Cyt28'* and *Gua2′-Cyt28*, of the DNA duplex pack against the side chains of Phe46 and Leu49 from adjacent crystallographic symmetry-related *so*NrtR molecules (Figure S3). These interactions may contribute to a more favorable crystal packing than when shorter nucleotides were used (see Experimental Procedures).

The 27 bp DNA duplex in the complex adopts a slightly distorted B form conformation (mean rise = 3.3Å, mean twist = 34.5°, mean roll = 2.6°, mean minor groove width = 5.9Å, and mean major groove width = 12.5Å). The helical axis of the DNA duplex is mostly straight but slightly bent at both ends, probably due to the intercrystal lattice stacking interactions with the adjacent *so*NrtR molecules. Each *so*NrtR monomer in the dimer interacts with the symmetry related half site of the palindromic NrtR box DNA in the same manner. Therefore the protein-DNA interactions between one *so*NrtR monomer and one half site of NrtR box will be described.

*so*NrtR interacts with DNA primarily through helix α7, termed "DNA recognition helix," and the β8-β9 hairpin wing of the wHTH domain. The α7 helix contacts DNA from the major groove side while the β hairpin wing contacts the minor groove (Figure 7A). The most prominent protein-DNA base interactions are contributed by Arg215 from the tip of the hairpin wing and

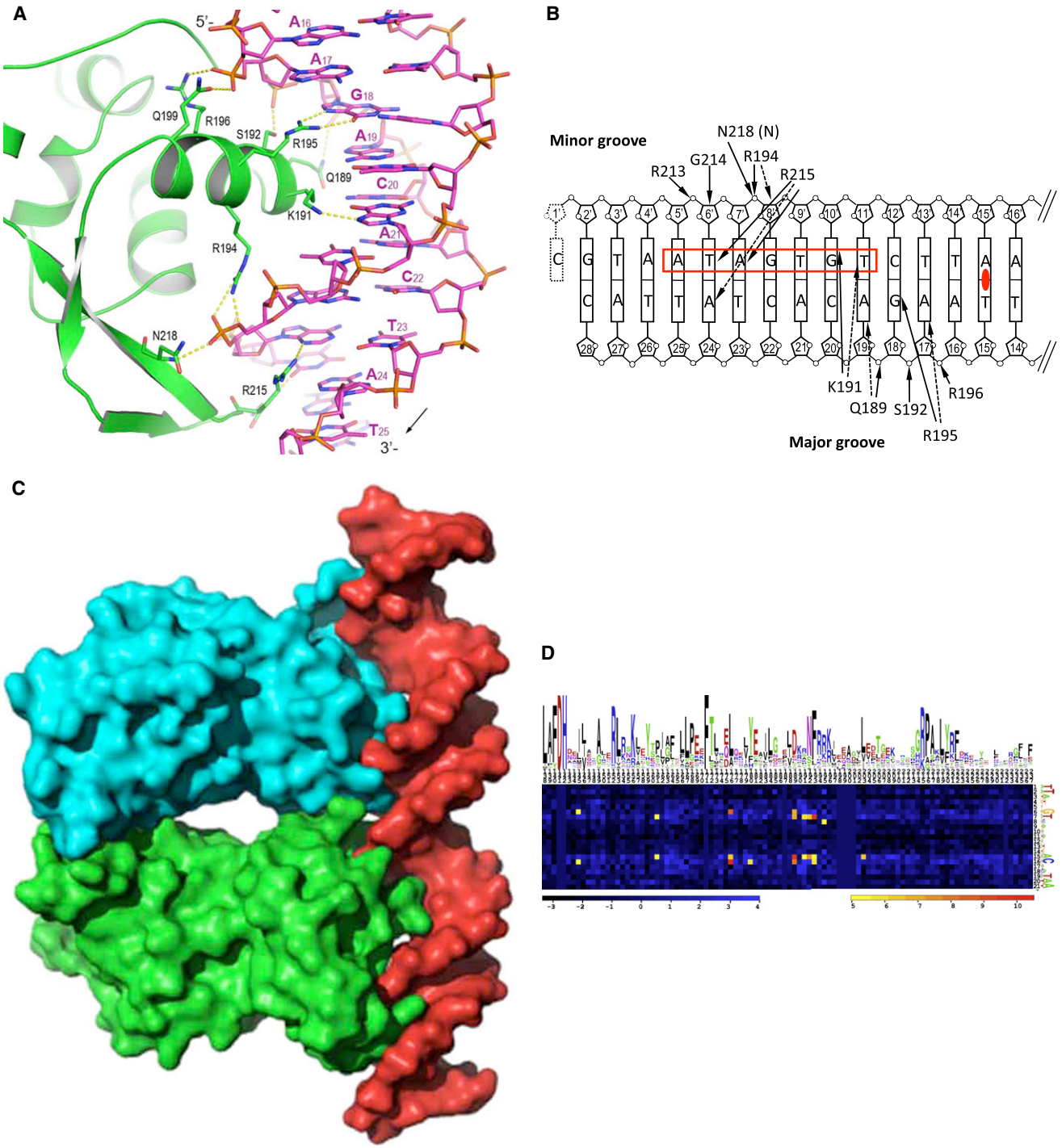

Figure 7. Interactions Between *so*NrtR and NrtR Box DNA

(A) Interactions between *so*NrtR (green) and one half site of *so*NrtR box DNA. Hydrogen bonds are indicated by dotted lines.

(B) Schematic illustration of *so*NrtR-DNA interactions. The ATA-n_2-GT consensus of NrtR box half site is boxed in red. Solid arrows indicate hydrogen bonds; dashed arrows van der Waals contacts. Primed deoxyribose denotes the complementary DNA strand. The dyad axis of DNA is indicated by a filled oval at the center of base pair *Ade15'-Thy15*.

(C) Molecular surface rendering of *so*NrtR dimer (green and cyan) and DNA duplex (red) in *so*NrtR-DNA complex.

(D) Heatmap of correlations between amino acid nucleotide pairs for NrtR proteins and their operators. Sequence logos of NrtR DNA-binding domains and NrtR box DNA are displayed above and to the right of the heatmap, respectively. The total height of the symbols in each position equals the positional information content, whereas the height of individual symbols is proportional to the positional amino acid/nucleotide frequency. The correlation scores are color ramped from yellow to red for amino acid nucleotide pairs with statistical significance Z scores greater than five.

Lys191 and Arg195 from the DNA recognition helix. The entire side chain of Arg215 is wedged in the minor groove of DNA. Hydrogen bonds are made between the backbone amide of Arg215 to O2 carbonyl of *Thy6*' and between the guadininium side chain of Arg215 and N3 of *Ade*7'. Arg215 is the most conserved residue in the NrtR family, where the only other substitution is Lys in a small subset of NrtR proteins (Figure S4). From the DNA recognition helix, the side chain of Arg195 forms two hydrogen bonds with *Gua18* base (to O6 and N7) and Lys191 side chain is hydrogen bonded to N7 of *Gua10'* (Figure 7A).

While there are relatively few sequence-specific interactions between *so*NrtR and NrtR box DNA, the DNA-interacting surface of *so*NrtR dimer is highly positively charged and several nonspecific polar interactions exist between the protein and DNA backbone phosphates. The side chains of residues Gln189, Ser192, Arg196, Arg194, and Arg213 contact the phosphates of *Ade*19', *Gua*18', *Ade*17', *Gua*8, and *Thy*6 nucleotide, respectively (Figures 7A and 7B). There are also extensive van der Waals interactions between *so*NrtR and DNA. The protein-DNA interface covers a total of 2392 Å^2 surface area, about ~1200 Å^2 from each wHTH domain. The shape of this DNA-interacting surface, composed from both *so*NrtR wHTH domains, is alternated with ridges and valleys that complement the major and minor grooves as well as the phosphate backbones of DNA duplex in a largely undistorted B form conformation (Figure 7C). The most conserved residue of the NrtR family, Arg215, also has the largest buried surface area (188 Å^2) upon DNA binding. Other residues with large buried surface upon DNA binding are Arg233 (113 Å^2), Lys191 (108 Å^2), Arg195 (92 Å^2), Gln189 (83 Å^2), Arg194 (94 Å^2), and Arg213 (75 Å^2). Therefore these residues contribute to DNA binding through not only specific hydrogen bonds but also van der Waals interactions.

Coevolution of NrtR Regulators and Their DNA Recognition Motifs

We previously predicted candidate NrtR-binding sites (NrtR boxes) in most microbial genomes that possess a NrtR transcription factor (Rodionov et al., 2008a). Different NrtR box consensus sequences were obtained for different NrtR subfamilies on the phylogenetic tree (Figure S5). Significant diversity in NrtR-binding motifs could be correlated with the amino acid sequences of NrtR wHTH domains. Using a multiple sequence alignment of 60 NrtR proteins (Figure S4) and the set of 115 candidate NrtR operators, we computed the correlation between amino acid sequences of NrtR wHTH domains and nucleotide sequences of their candidate DNA-binding sites (Figure 7D). We identified significantly correlated pairs of residues/nucleotides sites (21 pairs total). These sites included ten positions in NrtR proteins and five positions in DNA operators (Table S3). Among them, four residues (Gln189, Lys191, Ser192, and Arg195) lie on the DNA recognition helix and make contacts with DNA, five residues (Leu161, Leu176, His180, Phe193, and Leu203) form a part of the hydrophobic core of the wHTH domain, and one residue (Leu145) resides on the long α4 helix connecting the wHTH and Nudix domains (see Figure S6).

The first cluster of residues on the DNA recognition helix α7 (Gln189, Lys191, Ser192, and Arg195) may be important for specificity as both Lys191 and Arg195 make base-specific hydrogen bonds with DNA, while Gln189 makes the van der Waals contact with the *Ade19* base. In contrast, the most conserved Arg215 has a low correlation score, indicating that it is likely to be important for DNA-binding affinity and for recognizing the *Ade7* base conserved throughout NrtR family, rather than correlating with subfamily-specific NrtR box sequences. Interestingly, the second cluster of high scoring correlated residues comprises a part of the hydrophobic core of the wHTH domain (Figure S6**)**. How variations at these positions affect DNA-binding specificity is not straightforward to interpret, though they may possibly influence the orientation of the DNA recognition helix α7 and thus specificity. Further experimental investigations of divergent NrtR members are required to achieve a better understanding of their DNA-specificity determinants.

ADPR Modulates NrtR Repressor Function Through a Nudix Switch

ADPR binding triggers large conformational changes in several regions of *so*NrtR (Figure 8). First, the flexible N-terminal 18 residues become well structured upon ADPR binding and swap between the two subunits of the *so*NrtR dimer so that they interact with the ADPR molecule bound to the adjacent subunit. Aside from the N terminus, the most drastic conformational changes upon ADPR binding occur in the cross-over linker region connecting strands β6 and β7 (residues 109–125). We term this region "Nudix switch" for reasons discussed below. In apo *so*NrtR, an α helix (α2) exists in this region, whereas in the ADPR complex structure, the α2 helix completely unwinds and adopts an extended conformation (Figure 8). Notably, the average B factors of the α2 helix atoms in the apo *so*NrtR structure are higher than the rest of the Nudix domain (55 Å^2 versus 43 Å^2), suggesting that this region is intrinsically flexible. ADPR binding-induced conformational changes appear to stabilize the Nudix switch in the extended conformation as reflected in the better defined density and in the B factors that are comparable to the rest of the protein (35 Å^2). This Nudix switch region is equivalent to the flexible "L9 loop" in several other ADPRase and Nudix proteins (Bailey et al., 2002; Gabelli et al., 2001, 2002; Huang et al., 2008; Kang et al., 2003), in which two catalytic Asp residues are located at the tip of the loop (Figure S1). Large conformational changes usually occur in this region upon ligand binding to bring the aspartates close to the substrate (Figure 9). In ADPR-bound *so*NrtR, residue Ser121 at the tip of the loop, corresponding to one of the catalytic Asp of ADPRases, moves ~16 Å toward the ligand-binding pocket to interact with ADPR phosphate through a water molecule. Another noted ADPR binding-induced conformational change occurs at helix α1, which undergoes an upswing movement (~2.8 Å at the C terminus of the helix) (Figure 8). This movement enables the side chain of Lys76 to move about 5.5 Å and directly interact with the diphosphate group of ADPR (Figure 6). The concerted movements of the α1 helix and Nudix switch region extend the ADPR binding-induced conformational changes to the distal part of the Nudix domain that contacts the DNA-binding wHTH domain in the full-length *so*NrtR structure. Such a conformational change would result in close contacts (1.8–1.9 Å) between the C terminus of strand β6 (residues 109–111) and helix α5 of the wHTH domain (residues 163–167) (indicated by asterisk in Figure 8A). The wHTH domain would have to adopt a slightly different conformation in the presence of ADPR, which could

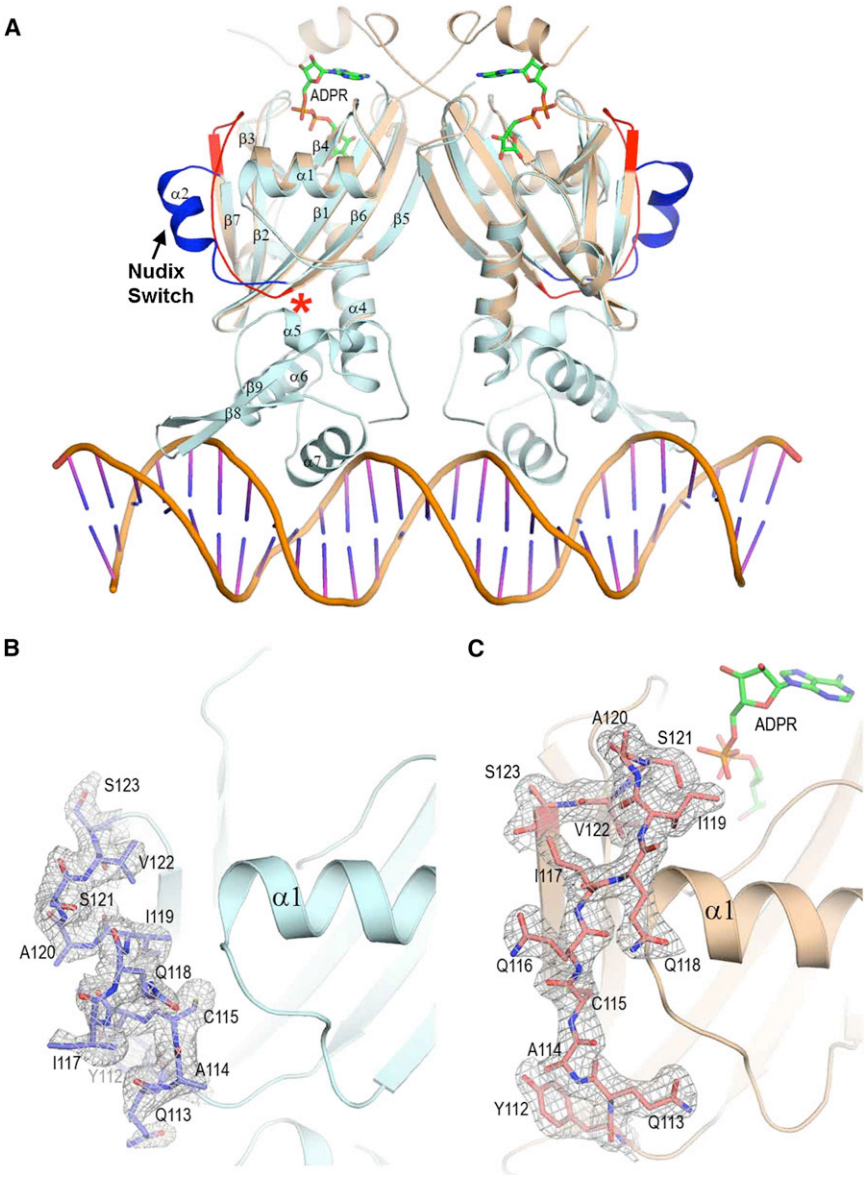

Figure 8. ADPR-Induced Conformational Changes in *so*NrtR

(A) Superposition of *so*NrtR N-terminal domain dimer in complex with ADPR (colored in beige) to *so*NrtR-DNA complex (protein in pale cyan and DNA in orange). The Nudix switch region is indicated by an arrow and highlighted in red and dark blue. The region where steric clash would occur is marked by a red asterisk.

(B and C) Electron densities of the Nudix switch region (shown as sticks) in the apo *so*NrtR (B) and ADPR-bound (C) structures. The densities are contoured at 1.0 σ.

be detrimental to its DNA-binding activity as the precise orientation of the two wHTH domains in *so*NrtR is important for creating a contiguous interface complementary to the DNA double helix. Additionally, based on the observation that ADPR binding increases susceptibility of the wHTH domain to protease cleavage (data not shown) and that our repeated attempts at obtaining full-length *so*NrtR-ADPR complex crystals have failed, it is also possible that ADPR-induced conformational changes may have a destabilizing effect on the wHTH domain and cause the domain to be more mobile.

DISCUSSION

We have previously predicted the existence of a novel family of transcriptional regulators, NrtRs, which may influence various aspects of NAD biosynthesis in many bacterial species (Rodionov et al., 2008a). In the present study, we carried out functional and structural characterization of NrtR from the γ-proteobacterium *S. oneidensis*, which was predicted to regulate the salvage/recycling of Nam by binding to the promoter region of the operon *prs-nadV* (Rodionov et al., 2008a). The existence of such an operon would allow a functional coupling of NadV-catalyzed NMN synthesis from Nam with the synthesis of PRPP, the co-substrate of NadV. The subsequent conversion of NMN to NAD would require its deamidation to NaMN by a yet uncharacterized NMN deamidase before adenylation by the NaMN-specific adenylyltransferase NadD. This interpretation is supported by the experimental verification of a NMN deamidase activity in crude cellular extracts of *S. oneidensis* (N.R., unpublished data).

In the present study we demonstrated that *nadV* is indeed cotranscribed with *prs* and that in vitro transcription of this operon is repressed by *so*NrtR binding to the predicted Nudix boxes in the promoter region. ADPR, pADPR, and NaADP bind NrtR with comparable affinity and abolish the repressor activity. While the physiological relevance of pADPR and NaADP in bacteria remains to be established, ADPR, along with Nam, is known to derive from enzymatic NAD hydrolysis. One possible source of ADPR is the reversible mono-ADP ribosylation of proteins that bacteria use as a mechanism to regulate endogenous protein functions. Well documented ADP ribosylation targets include dinitrogenase reductase in nitrogen-fixing bacteria (Ludden, 1994), RNA polymerase in *E. coli* cells infected with T4 phage (Goff, 1974), some bacterial glutamine synthetases (Ludden, 1994), membrane proteins involved in nutrient transport in *S. coelicolor* (Sugawara et al., 2002), and proteins controlling sporulation in *Bacillus subtilis* (Huh et al., 1996). Additionally, ADPR might be generated from acetyl-ADPR, the product of NAD-dependent protein deacetylases (CobB) of the sirtuin family that are present in various bacteria (Frye, 2000; Zhao et al., 2004). Finally, a mammalian

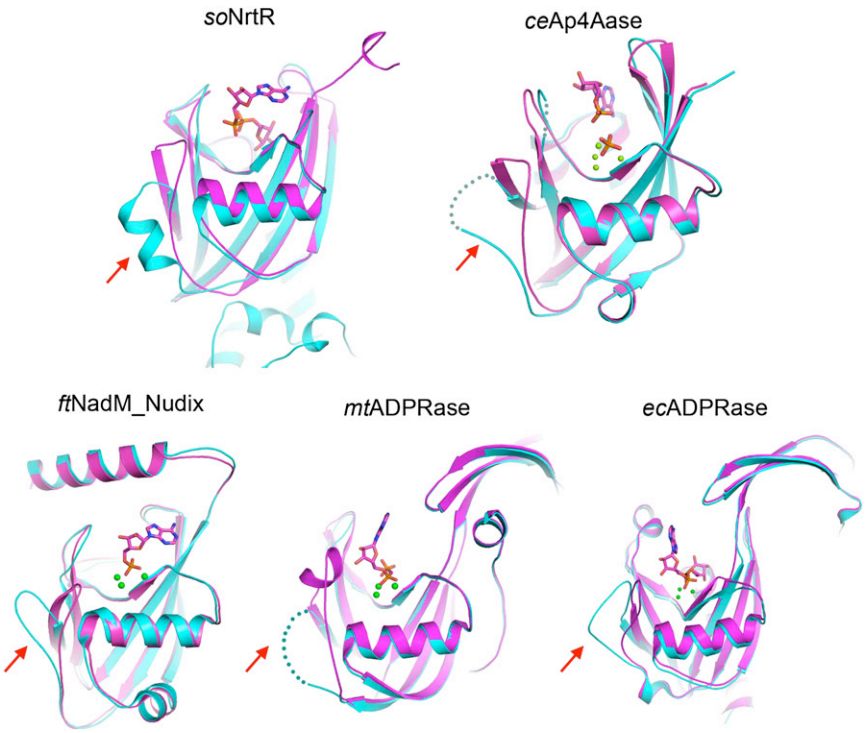

Figure 9. Nudix Switches in Various Nudix Proteins

Ligand binding-induced conformational changes in the following Nudix proteins are shown: *so*NrtR, *C. elegans* Ap4A hydrolase (*ce*Ap4Aase), the ADPRase domain of *Francisella tularensis* NadM_Nudix protein (*ft*NadM_Nudix), *M. tuberculosis* ADPRase (*mt*ADPRase), and *E. coli* ADPRase (*ec*ADPRase). The unliganded (cyan) and liganded (magenta) conformations for each protein are superimposed. The ligands are shown as sticks and metal ions as green balls. The disordered regions in some of the structures are shown as dotted lines. The corresponding Nudix switch region in each structure is indicated by a red arrow.

NAD glycohydrolase/ADPR cyclase (CD38) homologue is present in hemolytic streptococci (Kimoto et al., 2006;, Michos et al., 2006), and a NAD glycohydrolase activity has been detected in *Pseudomonas putida*, *B. subtilis,* and some *Mycobacterium* species, including *M. tuberculosis* (Everse et al., 1975; Gopinathan et al., 1964; Mather and Knight, 1972).

In the present work, we report for the first time the ADPR concentration in bacterial cells. In both *S. oneidensis* (this work) and *E. coli* (L. Sorci and A. Osterman, personal communication), the ADPR levels are in the low millimolar range, much higher than those determined in human cells, which range from 5 μM to 73 μM, depending on the cell type (Gasser and Guse, 2005; Heiner et al., 2006), and also higher than that in yeast cells (0.1 mM) (Tong et al., 2009). The presence of a consistently high ADPR pool is rather unexpected as free ADPR is considered a highly reactive, potentially toxic molecule that might cause nonenzymatic ADP-ribosylation of proteins (Jacobson et al., 1994). Since cellular ADPR levels are far above the binding constant of the metabolite toward NrtR, it is reasonable to assume that most NrtR proteins in cells are loaded with ADPR and thus do not repress the NAD biosynthetic genes. This assumption is consistent with the view that accumulation of ADPR in the cell is indicative of a very high NAD turnover and may be interpreted as a signal to replenish or maintain active NAD production.

The discovery of a distinct family of ADPR-dependent TFs revealed a new signaling function of ADPR in transcriptional regulation and further highlights the multifunctionality of this important metabolite. Besides transcriptional regulation, ADPR and related cyclic ADPR are important secondary messengers for Ca^{2+} signaling in vertebrate systems (Berger et al., 2004; Lee, 2001; Ying, 2007). In ADPR-gated TRPM2 (or LTRPC2) Ca^{2+} channels, a cytoplasmic Nudix domain is responsible for ADPR sensing (Kuhn et al., 2005; Perraud et al., 2001). In both cases where ADPR serves as a signaling molecule, the ancient and widespread Nudix hydrolase superfamily protein, in particular the ADPRase, was recruited for ADPR binding and signaling function.

Comparison of the structures of *so*NrtR-DNA and *so*NrtR_N-ADPR complexes provided a first glimpse of the structural mechanism underlying the regulatory function of a signaling Nudix domain. The unwinding of helix α2 and associated conformational changes in the Nudix switch region would generate a steric clash that interferes with the proper orientation of the wHTH domain, which may lead to the disruption of protein-DNA interaction. These conformational changes are reminiscent of those observed in several other Nudix proteins (Figure 9) and suggest that the Nudix switch is a particularly plastic structural element and may serve as a general conformational switch for signaling Nudix proteins.

Another prominent feature of NrtR regulators is their highly varied target DNA sequences in different bacterial species. The structures of *so*NrtR in complex with its cognate DNA operator reveals that *so*NrtR dimerizes primarily through interactions between its Nudix domains and that such dimerization brings the two wHTH DNA-binding domains into proximity to form a contiguous and symmetrical DNA-binding surface that complements the structure of B form DNA double helix. The binding specificity appears to be determined by a small number of specific interactions between the protein and conserved bases strategically placed along the DNA duplex. Notably, amino acid sequence alignment of NrtR wHTH domains (Figure S4) showed that although the overall sequence conservation of the domain is evident, none of the DNA-interacting residues observed in the *so*NrtR-DNA complex structure are strictly conserved among different NrtR subfamilies. This observation correlates with the highly varied NrtR box sequences present in different bacterial groups (Figure S5). In the loose consensus of the 21 bp NrtR box motif $_{(1)}$TTAnnGTnnnnnnnACnnTAA$_{(21)}$, *so*NrtR interacts specifically with the *Thy2*, *Ade3*, and *Gua6* bases (corresponding to *Thy6*, *Ade7*, and *Gua10* of the 28 nt

DNA used in the *so*NrtR-DNA complex crystallization; see Figure 7). A specific protein-base interaction also exists between Arg195 and *Gua14* (corresponding to *Gua18* in Figure 7), which is only conserved in a subset of NrtR operators. Statistically significant correlations between NrtR wHTH domain sequences and their DNA operators (Table S3) suggest the existence of subfamily-specific protein-DNA interactions, which enables each subfamily of NrtR to specifically recognize its own NrtR box motif.

EXPERIMENTAL PROCEDURES

Transcriptional Analysis of the *nrtR-prs-nadV* Region

Genomic DNA and RNA were isolated from *S. oneidensis* MR-1 cells grown in LB medium and collected at an OD of 2.0, using the DNeasy Blood and Tissue Kit (QIAGEN) and Trizol reagent (Sigma-Aldrich), respectively. Reverse transcription of total RNA was performed in the presence of random primers using the First Strand cDNA Synthesis kit (Bio Basic Inc.), after DNase I treatment, following the kit's instructions. PCR was performed on both genomic DNA and reverse transcribed RNA (Table S1).

In Vitro Transcription Assay

The DNA template of the target operon (*prs-nadV*) was generated by using primers prsfw and prsrev (Table S1) to amplify the 356 bp promoter region along with the first 440 bp of the *prs* gene of the *S. oneidensis* genomic DNA. The transcription reaction mixture contained the DNA template (20 nM), *so*NrtR, and the tested effectors at the indicated concentrations, in 40 mM HEPES (pH 7.5), 5 mM DTT, 5 mM MgCl, 2.5% glycerol, and 0.5 mg/ml acetylated BSA. After 20 min at room temperature, 20 U of RNase inhibitor and 0.05 U of *E. coli* σ^{70}-RNA polymerase holoenzyme (Epicenter Technologies) were added and after 15 min at 35°C, transcription was initiated by adding 25 μM of each nucleoside triphosphate. After 15 min incubation at 35°C, the template DNA was digested for 1 hr at 30°C with 2 U of DNase I (Sigma-Aldrich). mRNA transcripts were purified using the SV total RNA isolation system (Promega) and quantified after reverse transcription by real-time PCR amplifying *prs* gene internal regions (Table S1).

Determination of ADPR Concentration in *S. oneidensis*

S. oneidensis cells were grown in LB medium and collected at the late exponential phase (OD_{600} 2.0) by centrifugation (550 x *g*, 10 min, 4°C). About 4 × 10^{10} cells were resuspended in 0.66 ml of 100 mM potassium phosphate buffer, pH 6.0 and 0.34 ml of 1.2 M $HClO_4$. After lysis with an ultrasonic disruptor, cell debris was removed by centrifugation (10,000 x g, 10 min, 4°C). The supernatant was divided into two identical samples. To one sample (spiked sample), 8 nmol of ADPR were added. Samples were neutralized with 0.16 M K_2CO_3, kept on ice for 10 min, and centrifuged at 12,000 x g for 3 min. Supernatants were filtered and injected into the HPLC system equipped with a diode-array detector. The enzymatic degradation of ADPR was performed with nucleotide pyrophosphatase, as described in Heiner et al. (2006). The enzyme was then removed with a Microcon YM10 filter device (Millipore). HPLC separation was performed on a 12.5 cm Supelcosil LC-18-T, 3 μm particle size, reversed-phase column, at 16°C. Elution conditions were 12 min at 100% buffer A (100 mM potassium phosphate buffer [pH 6.0]), 8 min up to 12% buffer B (buffer A containing 20% methanol), 3 min up to 45% buffer B, and 3 min up to 100% buffer B, holding at 100% buffer B for 9 min and returning to 100% buffer A in 8 min. Flow rate was maintained at 1 ml/min. For NADH determination, cells were resuspended in 0.1 M NaOH and after lysis and centrifugation as described above, the supernatant was filtered with a Microcon YM10 filter device (Millipore). NADH concentration was determined in the filtrate spectrophotometrically at 340 nm, with pyruvate and lactate dehydrogenase.

Cell number measurement was performed by both direct microscopic counts and plate counts. The average volume of a *S. oneidensis* cell (0.2 μm^3) was calculated based on scanning electron microscope images (E.A. Hill, personal communication).

Crystallization, Data Collection, and Structure Determination

Crystallization of *so*NrtR was carried out using hanging drop vapor diffusion method. One microliter of *so*NrtR (20 mg/ml) was mixed with equal volume of reservoir solution containing 100 mM sodium citrate (pH 6.0) and 2.5 M sodium chloride and equilibrated against the reservoir at 20°C until crystal appeared. The crystals were transferred stepwise to a cryoprotection solution containing the original reservoir components and additional 30% glycerol and frozen in liquid nitrogen.

To obtain heavy atom derivatized *so*NrtR crystal, quick soaking methods (Dauter et al., 2000) were performed to introduce iodide ion in the crystal. *so*NrtR crystal was transferred stepwise into a soaking solution containing 1M NaCl, 1 M KI, and 100 mM sodium citrate (pH 6.0) and increasing the amount of glycerol up to 30% at 30 s each step and flash frozen in liquid nitrogen.

For the *so*NrtR-DNA cocrystallization trials, multiple oligodeoxynucleotides containing the NrtR box sequence with single 5′ overhang and lengths ranging from 25, 26, 27, and 28 nt were used. The best crystals were obtained with the 28 nt DNA of sequence 5′-$_{(1)}$CGTAATAGTGTCTTAAAGACACTATTAC$_{(28)}$ custom synthesized by Sigma-Genosys (nucleotides corresponding to the loose NrtR box consensus TTAnnGTnnnnnnnACnnTAA are underlined), which was annealed with its complementary strand to form a 27 bp duplex with one 5′-*Cyt* overhang. The protein-DNA complex was formed by mixing *so*NrtR dimer and annealed DNA duplex at a 1:1.5 molar ratio. The final protein concentration is 5 mg/ml. The *so*NrtR-DNA complex crystals were grown at 20°C after mixing equal volume of complex with reservoir solutions containing 0.1 M N-(2-acetamido) iminodiacetic acid (pH 5.5), 50 mM $MgCl_2$, and 8% PEG4000. The complex crystals were cryoprotected and frozen using a similar procedure as that for apo *so*NrtR crystals.

The N-terminal domain of *so*NrtR was generated by chymotrypsin treatment of purified full-length *so*NrtR in the presence of 200 μM ADPR overnight at 4°C. A single band around 15 kDa was observed in the SDS-PAGE after the treatment and mass spectral analysis indicated that the band contained residues 1–159 of *so*NrtR (denoted as *so*NrtR_N). *so*NrtR_N was then purified by Resource Q column (GE Healthcare) and concentrated to 20 mg/ml. For cocrystallization with ADPR (final concentration 5 mM), 1 μl of *so*NrtR_N-ADPR complex was mixed with equal volume of the well solution containing 100 mM Bis-Tris (pH 5.5), 20% PEG3350, and 200 mM ammonium acetate and equilibrated against the well for 2–4 days.

All data was collected at the X-ray facility at the University of Texas Southwestern Medical Center on a Rigaku FR-E rotating anode X-ray generator equipped with RAXIS IV^{2+} image plate detector. The data was processed with HKL2000 (Otwinowski and Minor, 1997). The statistics of all data sets are listed in Table 1. The apo *so*NrtR structure was determined by single isomorphous replacement/anomalous scattering phasing method while the N-terminal domain of *so*NrtR and *so*NrtR-DNA complex structures were determined by the molecular replacement method (see Supplemental Experimental Procedures).

ACCESSION NUMBERS

Atomic coordinates of apo *so*NrtR, *so*NrtR-DNA, and *so*NrtR_N-ADPR complexes have been deposited in the Protein Data Bank with accession codes 3GZ5, 3GZ6, and 3GZ8.

SUPPLEMENTAL DATA

Supplemental data include Supplemental Experimental Procedures, six figures, and three tables and can be found with this article online at http://www.cell.com/structure/supplemental/S0969-2126(09)00225-1.

ACKNOWLEDGMENTS

The authors wish to thank Drs. Andrei Osterman, Giulio Magni, Nick Grishin, and Silverio Ruggieri for helpful discussion; Lisa Kinch for critical reading of the manuscript; Adolfo Amici for technical assistance; and Eric Allen Hill for providing the *S. oneidensis* cell volume information. This work was supported by a Welch Foundation grant (I-5015) and in part by a National Institutes of

Table 1. Data Collection and Refinement Statistics

	Apo *so*NrtR KI Derivative	Apo *so*NrtR	*so*NrtR-DNA Complex	*so*NrtR_N-ADPR Complex
Data collection				
Space group	$P3_221$	$P3_221$	$P3_212$	$P2_12_12_1$
Cell dimensions				
a, *b*, *c* (Å)	75.30, 75.30, 172.53	75.16, 75.16, 172.51	159.58, 159.58, 73.07	63.05, 93.18, 132.50
Resolution (Å)	2.8	2.2	2.9	2.4
R_{sym} or R_{merge}	0.080 (0.590)[a]	0.039 (0.551)	0.097 (0.478)	0.050 (0.274)
$I/\sigma(I)$	28.14 (2.49)	39.17 (2.53)	20.68 (3.74)	27.39 (4.35)
Completeness (%)	99.9 (100.0)	99.6 (99.5)	98.4 (97.9)	99.0 (97.6)
Redundancy	4.7 (4.7)	4.7 (4.6)	6.1 (6.2)	4.6 (4.3)
Refinement				
Resolution (Å)		2.20	2.90	2.43
No. reflections		27,872	22,055	28,279
R_{work}/R_{free}		0.224/0.279	0.200/0.260	0.188/0.248
No. atoms				
Protein		3428	3544	4931
Ligand/ion		0/2	1107/1	144/0
Water		216	73	303
B factors (Å^2)				
Protein		50.96	34.22	32.46
Ligand/ion		66.78	42.95	32.02
Water		53.52	29.03	34.19
Rmsd				
Bond lengths(Å)		0.013	0.014	0.014
Bond angles (°)		1.59	1.87	1.79

[a] Values in parentheses are for the highest resolution shell.

Health grant (AI059146). The work of D.A.R. was partially supported by the "Integrated Biology of Shewanella" grant (PI J. Fredrikson) from the U.S. Department of Energy, Office of Biological and Environmental Research under the Genomics:GTL Program. M.S.G., A.B.R., and Y.D.K. were partially supported by grants from the Howard Hughes Medical Institute (55005610) and the Molecular and Cellular Biology program of the Russian Academy of Sciences (to M.S.G.).

Received: February 18, 2009
Revised: April 21, 2009
Accepted: May 6, 2009
Published: July 14, 2009

REFERENCES

Aravind, L., Anantharaman, V., Balaji, S., Babu, M.M., and Iyer, L.M. (2005). The many faces of the helix-turn-helix domain: transcription regulation and beyond. FEMS Microbiol. Rev. *29*, 231–262.

Bailey, S., Sedelnikova, S.E., Blackburn, G.M., Abdelghany, H.M., Baker, P.J., McLennan, A.G., and Rafferty, J.B. (2002). The crystal structure of diadenosine tetraphosphate hydrolase from *Caenorhabditis elegans* in free and binary complex forms. Structure *10*, 589–600.

Begley, T.P., Kinsland, C., Mehl, R.A., Osterman, A., and Dorrestein, P. (2001). The biosynthesis of nicotinamide adenine dinucleotides in bacteria. Vitam. Horm. *61*, 103–119.

Belenky, P., Christensen, K.C., Gazzaniga, F., Pletnev, A.A., and Brenner, C. (2009). Nicotinamide riboside and nicotinic acid riboside salvage in fungi and mammals. Quantitative basis for Urh1 and purine nucleoside phosphorylase function in NAD^+ metabolism. J. Biol. Chem. *284*, 158–164.

Berger, F., Ramirez-Hernandez, M.H., and Ziegler, M. (2004). The new life of a centenarian: signalling functions of NAD(P). Trends Biochem. Sci. *29*, 111–118.

Bessman, M.J., Frick, D.N., and O'Handley, S.F. (1996). The MutT proteins or "Nudix" hydrolases, a family of versatile, widely distributed, "housecleaning" enzymes. J. Biol. Chem. *271*, 25059–25062.

Dauter, Z., Dauter, M., and Rajashankar, K.R. (2000). Novel approach to phasing proteins: derivatization by short cryo-soaking with halides. Acta Crystallogr. D Biol. Crystallogr. *56*, 232–237.

Denu, J.M. (2005). The Sir 2 family of protein deacetylases. Curr. Opin. Chem. Biol. *9*, 431–440.

Everse, J., Everse, K.E., and Kaplan, N.O. (1975). The pyridine nucleosidases from *Bacillus subtilis* and *Neurospora crassa*. Isolation and structural properties. Arch. Biochem. Biophys. *169*, 702–713.

Frye, R.A. (2000). Phylogenetic classification of prokaryotic and eukaryotic Sir2-like proteins. Biochem. Biophys. Res. Commun. *273*, 793–798.

Gabelli, S.B., Bianchet, M.A., Bessman, M.J., and Amzel, L.M. (2001). The structure of ADP-ribose pyrophosphatase reveals the structural basis for the versatility of the Nudix family. Nat. Struct. Biol. *8*, 467–472.

Gabelli, S.B., Bianchet, M.A., Ohnishi, Y., Ichikawa, Y., Bessman, M.J., and Amzel, L.M. (2002). Mechanism of the *Escherichia coli* ADP-ribose pyrophosphatase, a Nudix hydrolase. Biochemistry *41*, 9279–9285.

Gasser, A., and Guse, A.H. (2005). Determination of intracellular concentrations of the TRPM2 agonist ADP-ribose by reversed-phase HPLC. J. Chromatogr. B Analyt. Technol. Biomed. Life Sci. *821*, 181–187.

Gerasimova, A.V., and Gelfand, M.S. (2005). Evolution of the NadR regulon in *Enterobacteriaceae*. J. Bioinform. Comput. Biol. *3*, 1007–1019.

Goff, C.G. (1974). Chemical structure of a modification of the *Escherichia coli* ribonucleic acid polymerase alpha polypeptides induced by bacteriophage T4 infection. J. Biol. Chem. *249*, 6181–6190.

Gopinathan, K.P., Sirsi, M., and Vaidyanathan, C.S. (1964). Nicotinamide-adenine dinucleotide glycohydrolase of *Mycobacterium tuberculosis* H37Rv. Biochem. J. *91*, 277–282.

Grose, J.H., Bergthorsson, U., and Roth, J.R. (2005). Regulation of NAD synthesis by the trifunctional NadR protein of *Salmonella enterica*. J. Bacteriol. *187*, 2774–2782.

Heiner, I., Eisfeld, J., Warnstedt, M., Radukina, N., Jungling, E., and Luckhoff, A. (2006). Endogenous ADP-ribose enables calcium-regulated cation currents through TRPM2 channels in neutrophil granulocytes. Biochem. J. *398*, 225–232.

Holbourn, K.P., Shone, C.C., and Acharya, K.R. (2006). A family of killer toxins. Exploring the mechanism of ADP-ribosylating toxins. FEBS J. *273*, 4579–4593.

Holley, E.A., Spector, M.P., and Foster, J.W. (1985). Regulation of NAD biosynthesis in *Salmonella typhimurium*: expression of nad-lac gene fusions and identification of a nad regulatory locus. J. Gen. Microbiol. *131*, 2759–2770.

Holm, L., and Sander, C. (1995). Dali: a network tool for protein structure comparison. Trends Biochem. Sci. *20*, 478–480.

Huang, N., Sorci, L., Zhang, X., Brautigam, C.A., Li, X., Raffaelli, N., Magni, G., Grishin, N.V., Osterman, A.L., and Zhang, H. (2008). Bifunctional NMN adenylyltransferase/ADP-ribose pyrophosphatase: structure and function in bacterial NAD metabolism. Structure *16*, 196–209.

Huh, J.W., Shima, J., and Ochi, K. (1996). ADP-ribosylation of proteins in *Bacillus subtilis* and its possible importance in sporulation. J. Bacteriol. *178*, 4935–4941.

Imai, S. (2009). Nicotinamide phosphoribosyltransferase (Nampt): a link between NAD biology, metabolism, and diseases. Curr. Pharm. Des. *15*, 20–28.

Jacobson, E.L., Cervantes-Laurean, D., and Jacobson, M.K. (1994). Glycation of proteins by ADP-ribose. Mol. Cell. Biochem. *138*, 207–212.

Kang, L.W., Gabelli, S.B., Cunningham, J.E., O'Handley, S.F., and Amzel, L.M. (2003). Structure and mechanism of MT-ADPRase, a nudix hydrolase from *Mycobacterium tuberculosis*. Structure *11*, 1015–1023.

Kimoto, H., Fujii, Y., Hirano, S., Yokota, Y., and Taketo, A. (2006). Genetic and biochemical properties of streptococcal NAD-glycohydrolase inhibitor. J. Biol. Chem. *281*, 9181–9189.

Koch-Nolte, F., Kernstock, S., Mueller-Dieckmann, C., Weiss, M.S., and Haag, F. (2008). Mammalian ADP-ribosyltransferases and ADP-ribosylhydrolases. Front. Biosci. *13*, 6716–6729.

Kuhn, F.J., Heiner, I., and Luckhoff, A. (2005). TRPM2: a calcium influx pathway regulated by oxidative stress and the novel second messenger ADP-ribose. Pflugers Arch. *451*, 212–219.

Lee, H.C. (2001). Physiological functions of cyclic ADP-ribose and NAADP as calcium messengers. Annu. Rev. Pharmacol. Toxicol. *41*, 317–345.

Ludden, P.W. (1994). Reversible ADP-ribosylation as a mechanism of enzyme regulation in procaryotes. Mol. Cell. Biochem. *138*, 123–129.

Magni, G., Amici, A., Emanuelli, M., Orsomando, G., Raffaelli, N., and Ruggieri, S. (2004). Enzymology of NAD^+ homeostasis in man. Cell. Mol. Life Sci. *61*, 19–34.

Marmorstein, R. (2004). Structure and chemistry of the Sir2 family of NAD^+-dependent histone/protein deactylases. Biochem. Soc. Trans. *32*, 904–909.

Mather, L.H., and Knight, M. (1972). A heat-stable nicotinamide-adenine dinucleotide glycohydrolase from *Pseudomonas putida* KB1. Partial purification and some properties of the enzyme and an inhibitory protein. Biochem. J. *129*, 141–152.

Michos, A., Gryllos, I., Hakansson, A., Srivastava, A., Kokkotou, E., and Wessels, M.R. (2006). Enhancement of streptolysin O activity and intrinsic cytotoxic effects of the group A streptococcal toxin, NAD-glycohydrolase. J. Biol. Chem. *281*, 8216–8223.

Otwinowski, Z., and Minor, W. (1997). Processing of X-ray diffraction data collected in oscillation mode. Methods Enzymol. *276*, 307–326.

Pantoliano, M.W., Petrella, E.C., Kwasnoski, J.D., Lobanov, V.S., Myslik, J., Graf, E., Carver, T., Asel, E., Springer, B.A., Lane, P., and Salemme, F.R. (2001). High-density miniaturized thermal shift assays as a general strategy for drug discovery. J. Biomol. Screen. *6*, 429–440.

Perraud, A.L., Fleig, A., Dunn, C.A., Bagley, L.A., Launay, P., Schmitz, C., Stokes, A.J., Zhu, Q., Bessman, M.J., Penner, R., et al. (2001). ADP-ribose gating of the calcium-permeable LTRPC2 channel revealed by Nudix motif homology. Nature *411*, 595–599.

Pohl, E., Haller, J.C., Mijovilovich, A., Meyer-Klaucke, W., Garman, E., and Vasil, M.L. (2003). Architecture of a protein central to iron homeostasis: crystal structure and spectroscopic analysis of the ferric uptake regulator. Mol. Microbiol. *47*, 903–915.

Ramakrishnan, V., Finch, J.T., Graziano, V., Lee, P.L., and Sweet, R.M. (1993). Crystal structure of globular domain of histone H5 and its implications for nucleosome binding. Nature *362*, 219–223.

Rodionov, D.A., De Ingeniis, J., Mancini, C., Cimadamore, F., Zhang, H., Osterman, A.L., and Raffaelli, N. (2008a). Transcriptional regulation of NAD metabolism in bacteria: NrtR family of Nudix-related regulators. Nucleic Acids Res. *36*, 2047–2059.

Rodionov, D.A., Li, X., Rodionova, I.A., Yang, C., Sorci, L., Dervyn, E., Martynowski, D., Zhang, H., Gelfand, M.S., and Osterman, A.L. (2008b). Transcriptional regulation of NAD metabolism in bacteria: genomic reconstruction of NiaR (YrxA) regulon. Nucleic Acids Res. *36*, 2032–2046.

Rossolillo, P., Marinoni, I., Galli, E., Colosimo, A., and Albertini, A.M. (2005). YrxA is the transcriptional regulator that represses de novo NAD biosynthesis in *Bacillus subtilis*. J. Bacteriol. *187*, 7155–7160.

Safo, M.K., Zhao, Q., Ko, T.P., Musayev, F.N., Robinson, H., Scarsdale, N., Wang, A.H., and Archer, G.L. (2005). Crystal structures of the BlaI repressor from *Staphylococcus aureus* and its complex with DNA: insights into transcriptional regulation of the bla and mec operons. J. Bacteriol. *187*, 1833–1844.

Sugawara, K., Dohmae, N., Kasai, K., Saido-Sakanaka, H., Okamoto, S., Takio, K., and Ochi, K. (2002). Isolation and identification of novel ADP-ribosylated proteins from *Streptomyces coelicolor* A3(2). Biosci. Biotechnol. Biochem. *66*, 2292–2296.

Tempel, W., Rabeh, W.M., Bogan, K.L., Belenky, P., Wojcik, M., Seidle, H.F., Nedyalkova, L., Yang, T., Sauve, A.A., Park, H.W., and Brenner, C. (2007). Nicotinamide riboside kinase structures reveal new pathways to NAD^+. PLoS Biol. *5*, e263.

Tong, L., Lee, S., and Denu, J.M. (2009). Hydrolase regulates NAD^+ metabolites and modulates cellular redox. J. Biol. Chem. *284*, 11256–11266.

Wilkinson, A., Day, J., and Bowater, R. (2001). Bacterial DNA ligases. Mol. Microbiol. *40*, 1241–1248.

Ying, W. (2007). NAD^+ and NADH in brain functions, brain diseases and brain aging. Front. Biosci. *12*, 1863–1888.

Zhao, K., Chai, X., and Marmorstein, R. (2004). Structure and substrate binding properties of cobB, a Sir2 homolog protein deacetylase from *Escherichia coli*. J. Mol. Biol. *337*, 731–741.